Implicit treatment of compositional flow

I. Garrido, E. Øian, M. Chaib, G.E. Fladmark and M.S. Espedal

Department of Mathematics, University of Bergen, Norway
E-mail: izaskun@mi.uib.no

In basin modeling the thermodynamics of a multicomponent multiphase fluid flux are computationally too expensive when derived from a cubic equation of state and the Gibbs equality constraints. In this article we present an alternative implicit molar mass formulation technique using binary mixture thermodynamics. The two proposed solution methods are based on a hybrid smoother, Gauss–Seidel–Galerkin at each time-step with analytical computation of the derivatives. The new algorithm overcomes the difficulty of choosing an optimal relaxation parameter and reduce significantly the numerical effort for the computation of the molar masses. Numerical results are presented which show significant improvements with respect to previous methods.

Keywords: binary mixture thermodynamics, compositional simulator, Galerkin, Gauss–Seidel, multiphase flow

1.   Introduction

The primary objective of basin simulation is to determine the possible locations of trapped hydrocarbons. Since the hydrocarbons use millions of years to migrate, the basin structure may change several times during the migration. It is not only the geometry and the geological data which cause difficulties. Compared to a reservoir model, a basin model includes many more unknowns due to the heat transport, chemical reactions and thermodynamics. Our work is based on a compositional simulator for secondary oil migration [10–12]. This 3D model gives full treatment of fractures and discontinuities of the medium, representing them by refined cells which contain the desired lithology [1,2].

In this work we have mostly used a simplified compositional model, named the binary mixture thermodynamics model [5]. The phase calculation is related to tables for dew and bubble points rather than fugacity calculations. In this model the oil and the gas components may partly be in both the oil and gas phases, while the water phase is treated separately.

The primary variables in our simulator, named `Athena`, are the temperature T, the water pressure p^{w}, and the molar masses N_{ν}, for each fluid component ν. The numerical model uses a control volume finite difference box-centered space discretization

technique [15] together with a *backward Euler* scheme for time discretization of the water pressure and temperature equations and an *explicit* solver for the mass equation. Recently a *fixed LGR* method has been successfully applied to cover discontinuities of the porous media [7]. This method does not only allow a full geometrical treatment of fault and matrix but it also serves as a middle step between the sequential and parallel processing, see [4] for a comparison with other simulators. Obviously, the above discretization introduces a CFL condition that severely restricts the time step [3]. In order to reduce the numerical effort, we propose two implicit numerical schemes to deal with a mass conservative dynamical behavior.

The main goal of this article is to illustrate the efficiency of the simulator with the new methods by numerical examples. For that purpose we consider different geometries and compare the numerical results obtained by the two implicit algorithms, based on a *Newton–Galerkin* with analytical derivatives, to those obtained by the *explicit* solver. For further information on Galerkin methods its motivation and implementation issues we refer to [14,16].

An outline of the paper is as follows. In section 2 we introduce the model to study. The numerical approximations to the primary variables temperature, water pressure and molar mass are given in sections 3, 4 and 5, respectively. The two implicit molar mass transport formulations are further described in section 6; other discretization schemes are given in [13]. Section 7 give some insight in the GS–Galerkin solver. Then, in section 8, we present some numerical results, and conclusions and future work summarize the paper in section 9.

2. The model

In this section we will give an introduction to the simulation model, which is implemented into the general compositional simulator `Athena`. It is based on a symmetric black oil model with the assumption that the water is always in water phase and any of the hydrocarbons may be in both gas and oil phase. For more information and details about compositional models we refer to [8,9].

For consistency reasons we introduce the following notation; the sub index v will denote any of the n_c fluid components, while the super index l denotes any of the three phases, oil, water or gas, in which the different components or fraction of them may exist. The water component is assumed to always be in water phase whilst the hydrocarbons are never in water phase. Besides, discretization indices will appear between brackets as subindices for the space and as super-indices for the time.

The molar mass conservation of a multicomponent multiphase fluid flowing through a porous media region V whose boundary is a closed surface S is given by the integral expression

$$\frac{\partial}{\partial t} \int_V m_v \, dV + \int_V \nabla \cdot \vec{m}_v = - \int_V q_v \, dV. \tag{1}$$

Here q_ν denotes the source/sink of molar mass density for each component ν with units mol/m^3 s. Besides, the molar mass flux and the density inside the region are respectively expressed as

$$\vec{m}_\nu = \sum_{l=\text{phase}} C_\nu^l \vec{v}^l \xi^l, \qquad (2)$$

$$m_\nu = \phi_\text{p} \sum_{l=\text{phase}} C_\nu^l S^l \xi^l. \qquad (3)$$

The entity C_ν^l denotes the mass fraction of component ν in phase l, and further

$\xi^l = \rho^l / M^l$ molar density of phase l, ρ^l mass density of phase l,

M^l the molecular weight of phase l, S^l saturation of phase l,

$\vec{v}^l$ the Darcy velocity of phase l, ϕ_p the rock porosity.

Energy conservation is enforced by the following integral expression for the heat flow equation

$$\frac{\partial}{\partial t} \int_V (\rho u)\, dV - \int_S (\underline{k}\nabla T) \cdot d\vec{S} = -\int_S h\rho\vec{u} \cdot d\vec{S} + \int_V q\, dV, \qquad (4)$$

where the capacity term and convective flux are

$$\rho u = \sum_{l=\text{g,o,w}} \phi_\text{p} S^l u^l \rho^l + u_\text{r}\rho_\text{r}(1 - \phi_\text{p}), \qquad (5)$$

$$h\rho\vec{u} = \sum_{l=\text{g,o,w}} h^l \rho^l \vec{v}^l. \qquad (6)$$

Here, the new parameters denote

T the temperature, $\underline{k}$ the bulk heat conductivity,

ρ_r mass density of rock, u_r internal energy of rock,

u^l internal energy of phase l, h^l enthalpy of phase l.

The volume balance method [17] imposes that the difference between the pore volume V_p and the volume of all phases

$$R = V_\text{p} - \sum_{l=\text{g,o,w}} V^l, \qquad (7)$$

has to be zero at any time. Besides, this residual volume is a function of the water pressure p^w the overburden pressure W and the integral of the molar mass for each component N_ν. Hence, the first order Taylor expansion of the residual $R(t+\Delta t)$ together

with the chain rule for partial differentiation of $\partial R(p^{\mathrm{w}}, W, N_v)/\partial t$ leads to the water pressure equation

$$\frac{\partial R}{\partial p^{\mathrm{w}}} \frac{\partial p^{\mathrm{w}}}{\partial t} + \sum_{v=1}^{n_c} \frac{\partial R}{\partial N_v} \frac{\partial N_v}{\partial t} = -\frac{R}{\Delta t} - \frac{\partial R}{\partial W} \frac{\partial W}{\partial t}. \tag{8}$$

In what follows, the numerical model will be derived from the discretization of the conservation equations (1), (4) and (8), using control volumes in space together with backward Euler in time.

3. Energy conservation

The integral of the source term of equation (4) will be treated explicitly for each control volume $V_{[i]}$

$$\int_{V_{[i]}} q \, \mathrm{d}V \approx Q_{[i]}. \tag{9}$$

Since the convective flux, given by equation (6), is small compared to the conductive flux, this term may be neglected or treated explicitly, in which case, the integral over each of the boundary surfaces is approximated by the value at the upstream control volume. Denoting by $I(i)$ the set of indices for the upstream volume V_i, the convective flux of equation (4) may be discretized as

$$\sum_k \int_{S_{[i,k]}} h\rho\vec{u} \cdot \mathrm{d}\vec{S} \approx \Phi,$$
$$\Phi_{[i]} = \sum_{in \in I(i)} \sum_{l=\mathrm{g,o,w}} h^l_{[i]} \rho^l_{[i]} \vec{v}^l_{[in]} S_{[i,k(in)]}, \tag{10}$$

where $S_{[i,k]}$ denotes the kth part of the surface boundary of the ith control volume, and $S_{[i,k(in)]}$ the part of the surface between the ith and inth control volumes.

The conductive heat flow for the ith control volume is approximated by

$$\int_{S_{[i]}} (\underline{k} \nabla T) \cdot \mathrm{d}\vec{S} \simeq -\sum_{j \in \mathcal{M}_i} \alpha_{[ij]} T_{[j]}, \tag{11}$$

where $\alpha_{[ij]}$ are the conductivity coupling coefficients, and the set $\mathcal{M}_i$ consists of the indices for all neighbors of the ith control volume including itself.

Finally, the capacity term is a function of the temperature

$$\frac{\partial}{\partial t} \int_V (\rho u) \, \mathrm{d}V \simeq \int_V \frac{\partial}{\partial t} (\rho u) \, \mathrm{d}V \simeq \int_V \left(\delta \frac{\partial T}{\partial t} \right) \mathrm{d}V, \tag{12}$$

where

$$\delta = \sum_{l=\mathrm{g,o,w}} \phi_{\mathrm{p}} S^l c^l \rho^l + c_{\mathrm{r}} \rho_{\mathrm{r}} (1 - \phi_{\mathrm{p}}). \tag{13}$$

The term $c_{\mathrm{r}} = \partial h_{\mathrm{r}}/\partial T$ denotes the rock specific heat capacity and $c^l = \partial h^l/\partial T$ the specific heat capacity of the phases. Even when the creation or disappearance of phases within each control volume may provoke large changes per phase, one would expect a more linear and smooth behavior over the addition of all phases. Space discretization is done by cell centered finite difference approximation, using an explicit value for the heat capacity at each control volume

$$\frac{\partial}{\partial t} \int_{V_{[i]}} (\rho u)\, \mathrm{d}V \simeq \delta_{[i]} \frac{\partial T_{[i]}}{\partial t}. \tag{14}$$

We have therefore substituted equations (9)–(11) and (14) into equation (4) to obtain the following finite control volume discretization of the energy

$$\delta_{[i]} \frac{\partial T_{[i]}}{\partial t} + \sum_{j \in \mathcal{M}_i} \alpha_{[ij]} T_{[j]} = -\Phi_{[i]} + Q_{[i]}, \tag{15}$$

which together with a backward Euler time discretization leads to a residual equation with matrix notation

$$0 = \mathcal{D}\big(\vec{T}^{[n+1]}\big) \frac{\vec{T}^{[n+1]} - \vec{T}^{[n]}}{\Delta t^{[n]}} + \mathcal{A}\big(\vec{T}^{[n+1]}\big)\vec{T}^{[n+1]} - \vec{b}\big(\vec{T}^{[n]}\big). \tag{16}$$

Here, $\Delta t^{[n]} = t^{[n+1]} - t^{[n]}$, $\mathcal{D} = \mathrm{diag}(\delta_{[i]})$, $\mathcal{A} = (\alpha_{[ij]})$ and $\vec{b} = (Q_{[i]} - \Phi_{[i]})$. Besides, both the convection and conduction terms have coefficients dominated by the rock temperature, which is almost constant, so that this equation may be linearized as

$$\mathcal{J}^{[n]}\Delta\vec{T}^{[n]} = -\vec{f}^{[n]}, \tag{17}$$

where $\Delta\vec{T}^{[n]} = (\vec{T}^{[n+1]} - \vec{T}^{[n]})$ and

$$\mathcal{J}^{[n]} = \frac{\mathcal{D}^{[n]}}{\Delta t^{[n]}} + \mathcal{A}^{[n]}, \qquad \vec{f}^{[n]} = \mathcal{A}^{[n]}\vec{T}^{[n]} - \vec{b}^{[n]}. \tag{18}$$

4. Treatment of the water pressure equation

Space discretization for the integral of equation (8) is done by the simple centered control volume evaluation

$$\delta_{[i]} \frac{\partial p_{[i]}^{\mathrm{w}}}{\partial t} + \sum_{v=1}^{n_c} \varepsilon_{v,[i]} \frac{\partial N_{v[i]}}{\partial t} = s_{[i]}, \tag{19}$$

where

$$\delta_{[i]} = \left(\frac{\partial R}{\partial p^{\mathrm{w}}}\right)_{[i]}, \qquad \varepsilon_{v,[i]} = \left(\frac{\partial R}{\partial N_v}\right)_{[i]}, \tag{20}$$

and $s_{[i]}$ denotes the value of the right-hand side of control volume.

In the discrete equation (19), the molar mass derivative may be expressed in terms of the water pressure. This approximation is obtained from equation (1), which using the divergence theorem reads

$$\frac{\partial N_\nu}{\partial t} + \int_S \sum_{l=\text{phase}} C_\nu^l \xi^l \vec{v}^l \cdot \vec{n} \, dS = Q_\nu, \tag{21}$$

where $\vec{n}$ is the unit outward normal vector to the boundary surface S, and Q_ν is the integral of the source term for component ν. Using the following expression for the Darcy velocity for phase l

$$\vec{v}^l = -\sum_{m=\text{g,o,w}} \underline{K} \frac{k_r^{lm}}{\mu^m} \left(\nabla p^m - \gamma^m \nabla d \right), \tag{22}$$

wher k_r^{lm} is the generalized relative permeability for coupled multiphase flow, $\underline{K}$ absolute permeability tensor, μ^m viscosity of the phase m, p^m fluid pressure of phase m, γ^m specific weight of phase m, d the depth, and the transmissibility tensors of each chemical component ν are

$$t_\nu^m = \sum_{l=\text{g,o,w}} C_\nu^l \xi^l \underline{K} \frac{k_r^{lm}}{\mu^m}. \tag{23}$$

Hence, the molar mass derivative in equation (21) may be rewritten as

$$\frac{\partial N_\nu}{\partial t} = \int_S \sum_{m=\text{g,o,w}} t_\nu^m \left(\nabla p^m - \gamma^m \nabla d \right) \cdot \vec{n} \, dS + Q_\nu. \tag{24}$$

Besides, the water pressure has been chosen as a primary variable so that the oil and gas phase pressures are given in terms of the water and the capillary pressures as

$$p^o = p^w + p_c^{ow}, \qquad p^g = p^o + p_c^{og}, \tag{25}$$

and part of the conductivity term is

$$\sum_{m=\text{g,o,w}} t_\nu^m \nabla p^m = \sum_{m=\text{g,o,w}} t_\nu^m \nabla p^w + \left(t_\nu^o + t_\nu^g \right) \nabla p_c^{ow} + t_\nu^o \nabla p_c^{og}. \tag{26}$$

Evaluation at the center of each control volume of the expression that results from substituting equation (26) into equation (24) leads to

$$\frac{\partial N_{\nu[i]}}{\partial t} = \sum_{j \in \mathcal{M}_i} t_{\nu[ij]} p_{[j]}^w + \Psi_{\nu[i]}, \tag{27.1}$$

$$\Psi_{\nu[i]} = Q_{\nu[i]} + \sum_{j \in \mathcal{M}_i} \left(t_{\nu[ij]}^g + t_{\nu[ij]}^o \right) p_{c[j]}^{ow} + t_{\nu[ij]}^g p_{c[j]}^{og} - g_{\nu[ij]} d_{[j]}, \tag{27.2}$$

where $t_{\nu[ij]} = \sum_l t^l_{\nu[ij]}$ denotes the discrete transmissibilities and $g_{\nu[ij]}$ the equivalent discrete gravitation. Substituting the molar mass derivative approximation given by equation (27) into equation (19) gives at each control volume

$$\delta_i \frac{\partial p^{\mathrm{w}}_{[i]}}{\partial t} + \sum_{j \in \mathcal{M}_i} \alpha_{[ij]} p^{\mathrm{w}}_{[j]} = \beta_{[i]}, \qquad (28)$$

with

$$\alpha_{[ij]} = \sum_{\nu=1}^{n_c} \varepsilon_{\nu[i]} t_{\nu[ij]}, \qquad \beta_{[i]} = s_{[i]} - \sum_{\nu=1}^{n_c} \varepsilon_{\nu[i]} \Psi_{\nu[i]}. \qquad (29)$$

Backward Euler time discretization of equation (28) gives a residual matrix equation for the water pressure

$$\mathcal{D}(\vec{p}^{\mathrm{w}[n+1]}) \frac{\vec{p}^{\mathrm{w}[n+1]} - \vec{p}^{\mathrm{w}[n]}}{\Delta t^{[n]}} + \mathcal{A}(\vec{p}^{\mathrm{w}[n+1]}) \vec{p}^{\mathrm{w}[n+1]} - \vec{b}(\vec{p}^{\mathrm{w}[n+1]}) = 0, \qquad (30)$$

with $\Delta t^{[n]} = t^{[n+1]} - t^{[n]}$. When solving this nonlinear equation with the *Newton–Rapson* method, we ensure that $\vec{p}^{\mathrm{w}[n(k)]} \to \vec{p}^{\mathrm{w}[n+1]}$ when $k \to \infty$, if our initial guess is "good" enough. Then, by using Taylor expansion of order one at $\vec{p}^{\mathrm{w}[n(k)]} + \Delta \vec{p}^{\mathrm{w}[n(k)]}$ we get the following equation for the increment

$$\mathcal{J}^{[n(k)]} \Delta \vec{p}^{\mathrm{w}[n(k)]} = -\vec{f}^{[n(k)]}, \qquad (31)$$

where $n(k)$ denotes the kth nonlinear *Newton–Rapson* iteration at the nth time level

$$\Delta \vec{p}^{\mathrm{w}[n(k)]} = \vec{p}^{\mathrm{w}[n(k+1)]} - \vec{p}^{\mathrm{w}[n(k)]},$$

$$\mathcal{J}^{[n(k)]} = \left(\frac{\partial \vec{f}}{\partial \vec{p}^{\mathrm{w}}} \right)^{[n(k)]} \simeq \frac{\mathcal{D}^{[n(k)]}}{\Delta t^{[n]}} + \mathcal{A}^{[n]}$$

and

$$\vec{f}^{[n(k)]} = \mathcal{D}^{[n(k)]} \frac{\vec{p}^{\mathrm{w}[n(k)]} - \vec{p}^{\mathrm{w}[n]}}{\Delta t^{[n]}} + \mathcal{A}^{[n]} \vec{p}^{\mathrm{w}[n(k)]} - \vec{b}^{[n]}.$$

Note that we do not update $\mathcal{A}$ and $\vec{b}$ for every iteration. The reason for this is that these calculations are rather expensive, and the accuracy we loose by this approximation may be neglected.

5. Implicit molar mass equations

Equation (1) is written as

$$\frac{\partial}{\partial t} N_\nu + \int_V \sum_l \nabla \cdot \left(C^l_\nu \xi^l \vec{v}^l \right) \mathrm{d}V = Q_\nu. \qquad (32)$$

Since the molar mass of phase l is $N^l = V^l \xi^l$, and denoting the inverse of volume for phase l by a^l equation (32) may be now expressed as

$$\frac{\partial}{\partial t} N_\nu + \int_V \sum_l \nabla \cdot \left(C_\nu^l a^l N^l \vec{v}^l \right) dV = Q_\nu. \tag{33}$$

Together with the divergence theorem, equation (33) is equivalent to

$$\frac{\partial}{\partial t} N_\nu + \int_S \sum_l C_\nu^l a^l N^l \vec{v}^l \cdot \vec{n} \, dS = Q_\nu, \tag{34}$$

where $\vec{n}$ is the unit outward normal vector to the boundary surface S. This mass transport equation shall be rewritten in terms of the molar mass of component ν in phase l, $N_\nu^l = C_\nu^l N^l$, which leads to

$$\frac{\partial}{\partial t} N_\nu + \int_S \sum_l a^l N_\nu^l \vec{v}^l \cdot \vec{n} \, dS = Q_\nu. \tag{35}$$

A finite control volume discretization is used to create the numerical model. Space discretization of equation (35) is done by cell centered finite difference approximation. The flux term is considered to be continuous across interfaces of area A, so that the surface integral of the normal component at the boundary of a given volume may be discretized as

$$\frac{\partial}{\partial t} N_{\nu[i]} + \sum_{is \in S_i} \sum_l \left(a^l N_\nu^l \right)_{[in]} \theta_{[is]}^l = Q_{\nu[i]}, \quad \theta_{[is]}^l = \left(\vec{v}^l \cdot \vec{n} \right)_{[is]} A_{[is]}. \tag{36}$$

The index *in* denotes the upstream volume with respect to each interface, *is*, of the ith control volume.

Time discretization of equation (36) is done by considering a backward Euler approximation of the derivative and by keeping the Darcy velocity and the phase volume constant at time $t^{[n]}$

$$\frac{N_{\nu[i]}^{[n+1]} - N_{\nu[i]}^{[n]}}{\Delta t^{[n]}} + \sum_{is \in S_i} \sum_l \left(a^{l[n]} N_\nu^{l[n+1]} \right)_{[in]} \theta_{[is]}^{l[n]} = Q_{\nu[i]}^{[n]}, \tag{37}$$

where $\Delta t^{[n]} = t^{[n+1]} - t^{[n]}$. The advection term in equation (37) will be treated implicitly when using *Newton–Rapson*. Thus, the molar mass of component ν in phase l may be expanded in terms of the molar mass of the different components as

$$N_\nu^{l[n(k+1)]} = N_\nu^{l[n(k)]} + \sum_\mu \left(\frac{\partial N_\nu^l}{\partial N_\mu} \right)^{[n(k)]} \Delta N_\mu^{[n(k)]},$$

$$\Delta N_\mu^{[n(k)]} = N_\mu^{[n(k+1)]} - N_\mu^{[n(k)]}, \tag{38}$$

where $N_\nu^{l[n(k)]} \to N_\nu^{l[n+1]}$ when $k \to \infty$ and index $n(k)$ denotes the kth nonlinear *Newton–Rapson* iteration at the nth time level. Therefore, the discrete molar mass trans-

port equation (37) of a chemical component ν flowing through a porous media region of a closed surface S, may be rewritten as

$$\frac{\Delta N_{\nu[i]}^{[n(k)]}}{\Delta t^{[n]}} + \sum_{is \in S_i} \sum_l \left(a^{l[n]} \sum_\mu J_{\nu\mu}^{l,[n(k)]} \Delta N_\mu^{[n(k)]} \right)_{[in]} \theta_{[is]}^{l[n]} = \beta_{\nu[i]}^{[n(k)]} \tag{39}$$

with $J_{\nu\mu}^{l,[n(k)]} = (\partial N_\nu^l / \partial N_\mu)^{[n(k)]}$ and right-hand side

$$\beta_{\nu[i]}^{[n(k)]} = Q_{\nu[i]}^{[n]} - \frac{N_{\nu[i]}^{[n(k)]} - N_{\nu[i]}^{[n]}}{\Delta t^{[n]}} - \sum_{is \in S_i} \sum_l \left(a^{l[n]} N_\nu^{l[n(k)]} \right)_{[in]} \theta_{[is]}^{l[n]}. \tag{40}$$

5.1. Full Jacobian matrix formulation

Considering multicomponent multiphase fluid flow, the matrix formulation of the molar mass equilibrium discrete equation (39) is of the form

$$\left(\frac{\mathcal{I}}{\Delta t^{[n]}} + \mathcal{A}^{[n(k)]} \right) \Delta \vec{N}^{[n(k)]} = \vec{b}^{[n(k)]}. \tag{41}$$

For a chemical system consisting of n_c components, located on a domain decomposed into n_{cv} control volumes

$$\left(\Delta \vec{N}^{[n(k)]} \right)_{\mu_j} = \Delta N_{\mu[j]}^{[n(k)]}, \qquad \left(\vec{b}^{[n(k)]} \right)_{\nu_i} = \beta_{\nu[i]}^{[n(k)]}, \quad \nu_i, \mu_j \in I, \tag{42.1}$$

$$I = \left\{ (1,1), \ldots, (n_c, 1), \ldots, (1, n_{cv}), \ldots, (n_c, n_{cv}) \right\}. \tag{42.2}$$

$\mathcal{I}$ is the identity matrix, and the matrix $\mathcal{A}$ has been ordered in n_{cv}^2 blocks each of them with n_c^2 entries of the form

$$\left(\mathcal{A}^{[n(k)]} \right)_{\nu_i, \mu_j} = \sum_l \alpha_{\nu_i, \mu_j}^{l[n(k)]}, \tag{43}$$

where for given a phase l, $j \in Im(i)$ denotes a cell which is upstream and is the interface between cells i and j, $\alpha_{\nu_i, \mu_i}^{ln[(k)]} = -\sum_{j \in Im(i)} \alpha_{\nu_i, \mu_j}^{ln[(k)]}$

$$\alpha_{\nu_i, \mu_j}^{ln[(k)]} = 0, \qquad\qquad\qquad j \notin Im(i), \tag{44a}$$

$$\alpha_{\nu_i, \mu_j}^{ln[(k)]} = a^{l[n]} \theta_{\nu[is]}^{l[n]} \left(\frac{\partial N_\nu^l}{\partial N_\mu} \right)_{[j]}^{n[(k)]}, \quad j \in Im(i). \tag{44b}$$

5.2. Sequential matrix formulation

The discrete molar mass equation (39) may be simplified considering the cross-derivatives between different components to be negligible. This assumption eliminates

the coupling and makes it possible to achieve greater computer efficiency by sequential solution of the following molar mass equations

$$\left(\frac{\mathcal{I}}{\Delta t^{[n]}} + \mathcal{A}_\nu^{[n(k)]}\right)\Delta\vec{N}_\nu^{[n(k)]} = \vec{b}_\nu^{[n(k)]}, \quad \nu = 1, \ldots, n_c, \tag{45}$$

where for a chemical system consisting of n_c components located on a domain decomposed into n_{cv} cells $i, j \in \{1, \ldots, n_{\text{cv}}\}$,

$$\left(\Delta\vec{N}_\nu^{[n(k)]}\right)_j = \Delta N_{\nu[j]}^{[n(k)]}, \qquad \left(\vec{b}_\nu^{[n(k)]}\right)_i = \beta_{\nu[i]}^{[n(k)]}, \tag{46}$$

$\mathcal{I}$ is the identity matrix and each matrix $\mathcal{A}_\nu$ has n_{cv}^2 entries $(\mathcal{A}_\nu)_{ij}^{[n(k)]} = \sum_l \alpha_{\nu_i,\nu_j}^{l[n(k)]}$, which are defined similarly to those of the full Jacobian.

Each set of equations (17), (31) and (41) or (17), (31) and (45), results in a compact numerical model, since they allow to find all the primary and secondary variables for the new time step.

6. Three phase system

The partial molar mass derivatives which appear in the molar mass discrete equations (41) and (45) are approximated based on binary system thermodynamics. Roughly speaking, the flux has three components: water, oil and gas which may be in either water, oil or gas phase. In particular, the oil and gas components should be viewed as the hydrocarbon components of the flux lumped into one gas and one oil component. This approximation at any fixed time t, generates for each phase $l = \text{w, o, g}$ the partial derivatives

$$\frac{\partial N_\nu^l}{\partial N_\mu}, \quad \nu, \mu = \text{w, o, g}, \tag{47}$$

where ν and μ denote the lumped (grouped) components.

6.1. Single hydrocarbon phase state

The derivatives under consideration (47) depend on the number of phases that are present in a control volume at that time. The single phase generates two subcases corresponding to being either only oil phase present or only gas phase present

$$N^{\text{g}} = 0: \quad N^{\text{o}} = N_{\text{o}} + N_{\text{g}}; \qquad N_{\text{o}}^{\text{o}} = N_{\text{o}} \quad \text{and} \quad N_{\text{g}}^{\text{o}} = N_{\text{g}},$$

$$N^{\text{o}} = 0: \quad N^{\text{g}} = N_{\text{o}} + N_{\text{g}}; \qquad N_{\text{o}}^{\text{g}} = N_{\text{o}} \quad \text{and} \quad N_{\text{g}}^{\text{g}} = N_{\text{g}},$$

leading to the unit matrix

$$\begin{bmatrix} \dfrac{\partial N_{\text{o}}^l}{\partial N_{\text{o}}} & \dfrac{\partial N_{\text{g}}^l}{\partial N_{\text{o}}} \\[3mm] \dfrac{\partial N_{\text{o}}^l}{\partial N_{\text{g}}} & \dfrac{\partial N_{\text{g}}^l}{\partial N_{\text{g}}} \end{bmatrix} = \mathcal{I}. \tag{48}$$

6.2. Two hydrocarbon phase state

Considering a control volume with both oil and gas phase present, the partial derivatives may be expressed in terms of bubble $\beta(p^{\mathrm{w}}, T)$ and dew point $\alpha(p^{\mathrm{w}}, T)$,

$$\alpha = \frac{N_{\mathrm{o}}^{\mathrm{g}}}{N^{\mathrm{g}}}, \qquad \beta = \frac{N_{\mathrm{o}}^{\mathrm{o}}}{N^{\mathrm{o}}}, \quad N^{\mathrm{g}} = N_{\mathrm{o}}^{\mathrm{g}} + N_{\mathrm{g}}^{\mathrm{g}}, \ N^{\mathrm{o}} = N_{\mathrm{o}}^{\mathrm{o}} + N_{\mathrm{g}}^{\mathrm{o}}. \tag{49}$$

In order to simplify the calculations it will be useful to introduce the molar fraction of oil phase in the system

$$z^{\mathrm{o}} = \frac{N^{\mathrm{o}}}{N}, \quad N = N_{\mathrm{o}} + N_{\mathrm{g}} = N^{\mathrm{o}} + N^{\mathrm{g}}, \tag{50}$$

and the molar fraction of oil component $z_{\mathrm{o}} = N_{\mathrm{o}}/N$. Besides, z_{o} and z^{o} may also be expressed in terms of the bubble and dew points since

$$z_{\mathrm{o}} = \frac{N^{\mathrm{o}}\beta + N^{\mathrm{g}}\alpha}{N}, \tag{51}$$

and it is a straight forward computation to check that

$$\frac{N^{\mathrm{o}}}{N} = \frac{(N^{\mathrm{o}}\beta + N^{\mathrm{g}}\alpha)/N - \alpha}{\beta - \alpha},$$

the left-hand side of which is z^{o}, as given in (50), and substituting (51) in the right-hand side gives the desired expression

$$z^{\mathrm{o}} = \frac{z_{\mathrm{o}} - \alpha}{\beta - \alpha}. \tag{52}$$

Once the variables α, β have been defined, it is necessary to give a suitable expression of the quantities to differentiate

$$N_{\mathrm{o}}^{\mathrm{o}} = \beta N^{\mathrm{o}} = \beta z^{\mathrm{o}} N, \qquad\qquad N_{\mathrm{g}}^{\mathrm{g}} = (1 - \alpha)N^{\mathrm{g}} = (1 - \alpha)(1 - z^{\mathrm{o}})N, \quad \text{(53a)}$$
$$N_{\mathrm{o}}^{\mathrm{g}} = \alpha N^{\mathrm{g}} = \alpha(1 - z^{\mathrm{o}})N, \qquad N_{\mathrm{g}}^{\mathrm{o}} = (1 - \beta)N^{\mathrm{o}} = (1 - \beta)z^{\mathrm{o}}N. \quad \text{(53b)}$$

The calculation of the derivatives for (53) with respect to either the oil molar mass or the gas molar mass is now a straightforward task after substituting z^{o} for its corresponding value as given in (52) and recalling from $z_0 = N_0/N$ that

$$\frac{\partial z_{\mathrm{o}}}{\partial N_{\mathrm{o}}} = \frac{1 - z_{\mathrm{o}}}{N}, \qquad \frac{\partial z_{\mathrm{o}}}{\partial N_{\mathrm{g}}} = \frac{-z_{\mathrm{o}}}{N}. \tag{54}$$

To simplify the description, a sketch of these analytical derivatives follows

$$\begin{bmatrix} \dfrac{\partial N_{\mathrm{o}}^{\mathrm{o}}}{\partial N_{\mathrm{o}}} & \dfrac{\partial N_{\mathrm{g}}^{\mathrm{o}}}{\partial N_{\mathrm{o}}} \\[2mm] \dfrac{\partial N_{\mathrm{o}}^{\mathrm{o}}}{\partial N_{\mathrm{g}}} & \dfrac{\partial N_{\mathrm{g}}^{\mathrm{o}}}{\partial N_{\mathrm{g}}} \end{bmatrix} = \begin{bmatrix} \dfrac{(1 - \alpha)\beta}{\beta - \alpha} & \dfrac{(1 - \alpha)(1 - \beta)}{\beta - \alpha} \\[4mm] -\dfrac{\alpha\beta}{\beta - \alpha} & -\dfrac{\alpha(1 - \beta)}{\beta - \alpha} \end{bmatrix}, \tag{55a}$$

$$
\begin{bmatrix} \dfrac{\partial N_o^g}{\partial N_o} & \dfrac{\partial N_g^g}{\partial N_o} \\[2ex] \dfrac{\partial N_o^g}{\partial N_g} & \dfrac{\partial N_g^g}{\partial N_g} \end{bmatrix} = \begin{bmatrix} -\dfrac{\alpha(1-\beta)}{\beta-\alpha} & -\dfrac{(1-\alpha)(1-\beta)}{\beta-\alpha} \\[2ex] \dfrac{\alpha\beta}{\beta-\alpha} & \dfrac{(1-\alpha)\beta}{\beta-\alpha} \end{bmatrix}.
\tag{55b}
$$

It is easy to verify these calculations since the sum of the two matrices above is the identity matrix, as it should be.

7.   Numerical solver

The following algorithm for solving each of the residual equations that result from the finite volume discretization at each Newton step is a relaxation method. Considering the grid to be parallel to the axis, the discretized equations in our system have a special matrix structure, $\mathcal{J}\Delta\vec{x} = \vec{y}$, where

$$
\mathcal{J} = \begin{bmatrix} T_{1,1} & D_{1,2} & & & \\ D_{2,1} & T_{2,2} & D_{2,3} & & \\ \ddots & \ddots & \ddots & & \\ & D_{n-1,n-2} & T_{n-1,n-1} & D_{n-1,n} \\ & & D_{n,n-1} & T_{n,n} \end{bmatrix}.
$$

When the grid is refined in just one of the three dimensions, the discretization is equivalent to a 1D approximation so that the entries of the Jacobian $\mathcal{J}^1$ are all scalars. However, if the grid is refined in two of the dimensions, the Jacobian $\mathcal{J}^2$ is block-tridiagonal with D diagonal matrices and T of the form $\mathcal{J}^1$; in agreement with a 2D discretization. Finally, in the full 3D case the Jacobian is a 7-diagonal matrix where D are diagonal matrices, and each T has the same shape as $\mathcal{J}^2$. Thus, in the full 3D case the system has blocks of lines of the general form

$$
\mathcal{A}_m \vec{x} = \vec{y}_m, \quad m = 1, \dots, M,
\tag{56}
$$

$$
\mathcal{A}_m = (D_{m,m_1} + D_{m,m_2} + T_{m,m} + D_{m,m_3} + D_{m,m_4}),
\tag{57}
$$

where $D_{m,*}$ and $T_{m,m}$ are respectively diagonal and three-co-diagonal matrices of dimension $m_s \times m_s$, while $\vec{y}_m$ is an m_s-dimensional data vector, being m_s the number of control volumes at the mth geological line in a given dimension. The steps when solving the general system (56) are smoothing, restriction and prolongation.

7.1. The Gauss–Seidel as smoother

Assuming anisotropic media where the heterogeneity varies more along one dimension than another, the system may be reordered so that the strongest variation occurs in the dimension that determines the size of each line-block (56). Since successive over-relaxation is always a good smoother, this method relaxes a whole block of lines simultaneously using Block-GS, which involves splitting the sparse matrices that arise

from the finite volume approximation in a set of systems. This set, (56) is solved using a block Gauss–Seidel method

$$T_{m,m}\vec{x}_m^{[m]} = \vec{y}_m - D_{m,m_1}\vec{x}_{m_1}^{[m-1]} - D_{m,m_2}\vec{x}_{m_2}^{[m-1]} - D_{m,m_3}\vec{x}_{m_3}^{[m-1]} - D_{m,m_4}\vec{x}_{m_4}^{[m-1]}, \quad (58)$$

where the superindices indicate that, in the current sequential formulation, the solution of each block depends on the solution of the previous one. Each system (58) corresponds to one geological line in the given dimension and it is solved by forward elimination and over-relaxed backward substitution. After solving each of these blocks, $m = 1, \ldots, M$, the generalized GS will iterate until a solution is found [6,18].

The downside of this method is that it only works for diagonal dominant matrices and that its convergence rate is highly dependent on the relaxation parameters. The matrices resulting from our residual formulation are always strict diagonal dominant for small enough time steps, but without an optimal choice of relaxation parameters, the GS method will be render inefficient.

7.2. Galerkin acceleration

The convergence of the block GS algorithm may be accelerated by using a coarse mesh re-balancing technique based on the Galerkin variational method. Consider that the linear equations (56) have been solved with the GS (see (58)) and define the set of basis functions

$$\vec{\Phi}_m \in \Re^{m_s}, \quad m = 1, \ldots, M, \quad (59)$$

consisting of only zero elements except for unit elements at entries corresponding to the mth block. Using the test function $\vec{z}$ given by

$$\vec{z} = \vec{x} + \sum_{m=1}^{M} \vec{d}_m \vec{\Phi}_m, \quad (60)$$

where $\vec{z}$ is the solution to the variational formulation

$$\langle \vec{\Phi}_m, \mathcal{J}\vec{z} \rangle = \langle \vec{\Phi}_m, \vec{y} \rangle, \quad m = 1, \ldots, M; \quad (61)$$

it yields the following equations for the unknowns $\vec{d}_m$

$$\widehat{\mathcal{J}}\vec{d}_m = \hat{\vec{y}}, \quad m = 1, \ldots, M, \quad (62)$$

where $\widehat{\mathcal{J}}_{m,n} = \langle \vec{\Phi}_m, \mathcal{J}\vec{\Phi}_n \rangle$ is a matrix tridiagonal with fringes and $\hat{\vec{y}} = \langle \vec{\Phi}_m, \vec{y} - \mathcal{J}\vec{x} \rangle$. The sparse structure of $\widehat{\mathcal{J}}$ may be exploited by solving the system with blockwise forward elimination and backward substitution.

7.3. Gauss–Seidel–Galerkin

Block Gauss–Seidel has proven to be an efficient smoother for many problems. However, its convergence is slow and depends on two relaxation parameters: outer relaxation parameter, which relates block solutions to each other, and inner relaxation
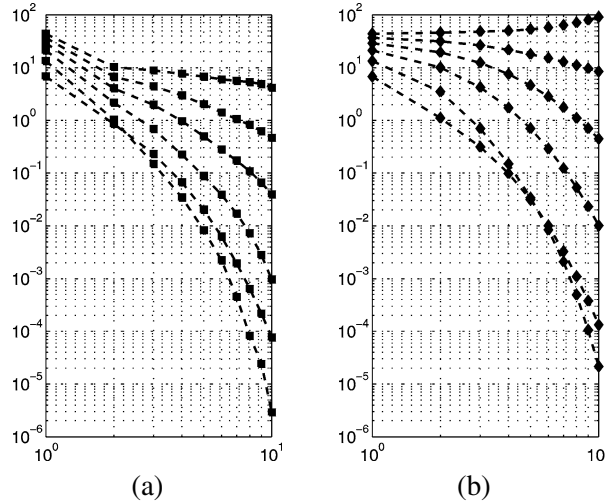
Figure 1. Solution error with respect to the number of solver iterations, $it = 1 : 10$, considering (a) the full GS–Galerkin, and (b) GS. The error increases proportionally to the relaxation parameter, $w = 0.9 : 0.2 : 1.9$.

parameter which is a smoothing parameter within each block. In particular, the choice of the outer parameter is of special relevance for convergence since it affects the whole matrix. However, the Galerkin acceleration acts as a physical smoother for the GS solution, diminishing the effect of different parameter choices. Considering a random matrix where we impose diagonal dominance and simulate a low permeability area by decreasing the connectivity in a CV block, we may see from figure 1 that the GS looses convergence as the relaxation parameter $w \to 2$, while GS–Galerkin is more robust with respect to the choice of w.

8.   Numerical examples

This section will illustrate with two different examples the efficiency of the two novel implicit molar mass formulations: full Jacobian and sequential Jacobian, within the `Athena` simulator. As expected, it will be seen that the new implicit formulations are particularly useful to avoid the time step constraints that the CFL condition imposes when using the explicit formulation. Additionally, the robustness of the implicit methods as function of the time step will be studied.

8.1. A first example: The dome

Before proceeding with the numerical experiments, the geological domain and boundary conditions shall be described. The three-dimensional domain has 50 m depth on the ends, and a size of 1000 m × 100 m × 70 m. There are four different layers in the z direction: shale, sandstone, shale and sandstone again. The lithology for the sandstone has a porosity of $\phi = 0.5$ and a permeability of $K_x = 500$ mD, $K_y = 500$ mD
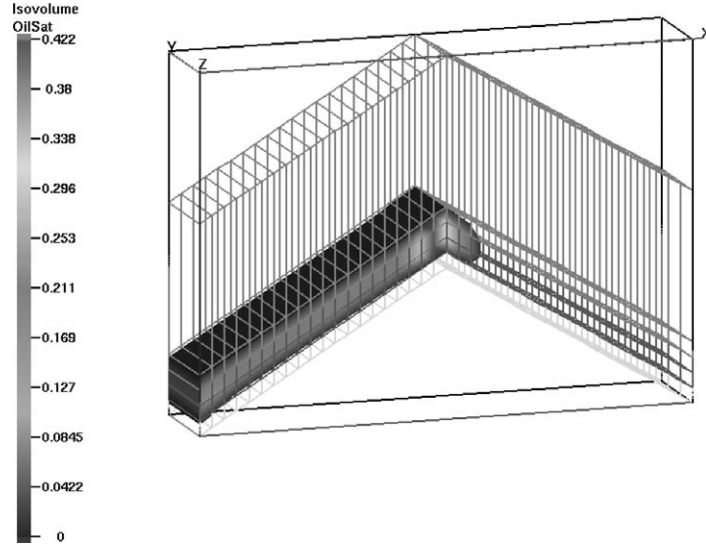
Figure 2. Oil migration simulated by `Athena` for $100y$ with $0.0047y$ as time step.

and $K_z = 500$ mD while the corresponding values for the shale are $\phi = 0.5$ and $K_x = 5 \cdot 10^{-6}$ mD, $K_y = 5 \cdot 10^{-6}$ mD and $K_z = 5 \cdot 10^{-6}$ mD. The boundary conditions consist of an explicitly given flux of oil and gas with value $5 \cdot 10^{-5}$ mol/m^2 s going inwards on the left-hand side and an outwards water flux with value $6.5 \cdot 10^{-4}$ mol/m^2 s in the right-hand side. There are also temperature boundary conditions of 450 K at the top and 460 K at the bottom. The domain is uniformly subdivided in each direction as is shown in figure 2, which serves as an illustration of the `Athena` output.

In order to validate the two new implicit methods for the molar mass equations, they will be compared to the explicit solver. The `Athena` simulator is run for each of these three methods and the time step has been set to be small enough for the CFL condition to remain inactive in the explicit case. For these small time steps the reference solution given by the explicit solver is graphically indistinguishable from the solution obtained with the implicit methods. Thus, the relevant factor to analyze is how the solution of the implicit formulation varies as the maximum allowed time step increases. Given an implicit solver, we shall compare the hydrocarbon saturations $S^l, l = $ o, g, that result from simulations with different maximum value of the time steps. The error norm is chosen to be $\|S^l_{\Delta t} - S^l_{\Delta t_0}\|_{L_1}$ with time steps Δt, that double from $\Delta t = 0.00235y$ until $0.6y$ using as reference solution $S_{\Delta t_0}$, the one obtained with maximum time step $\Delta t_0 = 0.0006y$. Figure 3 shows that the full Jacobian is more robust than the sequential method as it should be expected, since in the sequential formulation the cross derivatives have been neglected. Even when the error is bounded below 10%, the sequential formulation shows an erratic convergence rate for time steps bigger than $0.0376y$, where, according to table 1, the explicit method would impose severe CFL conditions. Concerning the computational time, it may be read in table 1 that whilst the CPU time for the explicit method remains bounded above a quantity close to that obtained when the CFL condition
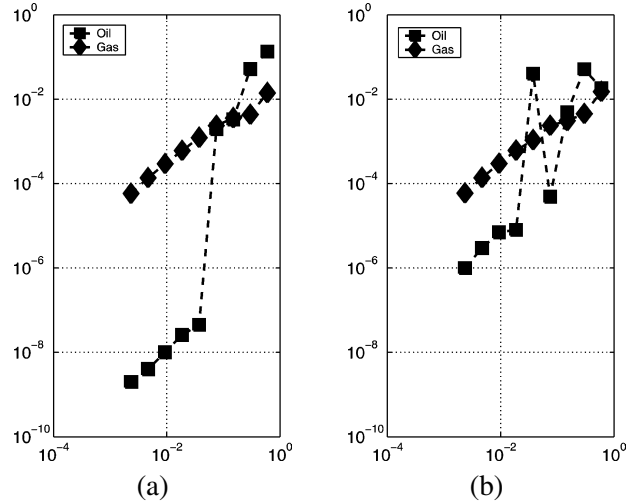
Figure 3. `Athena` simulation of $100y$; the L_1 error in saturations, against maximum allowed time step, $\Delta t \in (0.00235y, 0.6y)$. (a) Full Jacobian solution, and (b) sequential Jacobian.

Table 1
CPU time statistics: `Athena` simulation of $100y$ with three solvers.

max Δt	0.0094	0.0188	0.0376	0.0752	0.15	0.3	0.6
Exp.	x	$\dfrac{x}{2}$	$\dfrac{x}{2}$	$\dfrac{x}{2}$	$\dfrac{x}{2}$	$\dfrac{x}{2}$	$\dfrac{x}{2}$
Seq.	y_s	$\dfrac{y_s}{2}$	$\dfrac{y_s}{4}$	$\dfrac{y_s}{8}$	$\dfrac{y_s}{16}$	$\dfrac{y_s}{32}$	$\dfrac{y_s}{64}$
Jac.	y_j	$\dfrac{y_j}{2}$	$\dfrac{y_j}{4}$	$\dfrac{y_j}{8}$	$\dfrac{y_j}{16}$	$\dfrac{y_j}{32}$	$\dfrac{y_j}{64}$

becomes for the first time active, the CPU time for both implicit methods decreases at a rate inversely proportional to the maximum allowed time step. Even when the respective CPU times at small time steps x, y_s and y_j depend on implementation factors, in our particular simulations they do have similar values as expected from the analytical nature of the implicit formulation.

8.2. A highly nonlinear model

In this subsection numerical results for a full 3D treatment of a domain with a fault shall be described. The domain has a size of [8.75, 1, 8.75] m × 10 m × [7.5, 2.5, 10] m and 8 m depth at the left end. It has three different layers both in the x and in the z direction, shale, sandstone and shale again. The lithologies have the same values as those given in section 8.1 and the boundary conditions consist of an explicitly given flux of oil and gas with value $0.2 \cdot 10^{-4}$ mol/m^2 s going inwards on the left-hand side and an outwards water flux with value $2.5 \cdot 10^{-4}$ mol/m^2 s on the right-hand side. Some results of this model simulation with `Athena` are shown in figure 4.
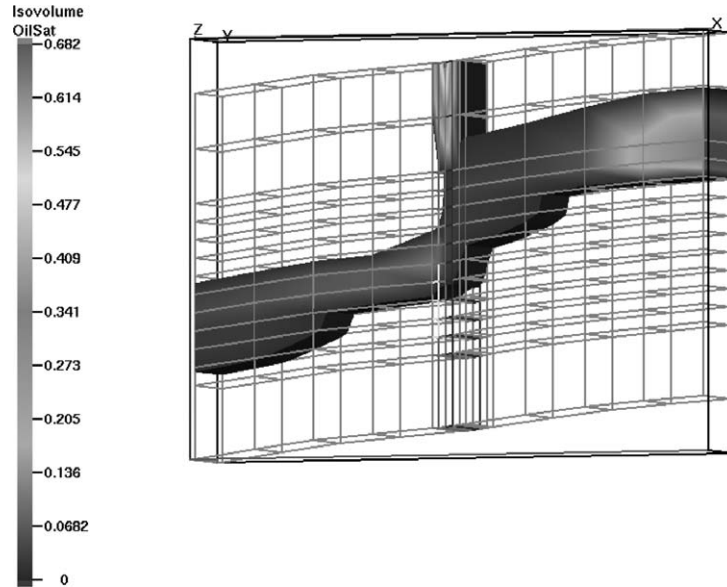
Figure 4. Oil migration simulated by `Athena` for $20y$ with $0.0047y$ as time step.

Table 2
CPU time statistics: `Athena` simulation of $20y$ with three solvers.

max Δt	0.00235	0.0047	0.0094	0.0188	0.0376	0.0752	0.15
Exp.	x	$\dfrac{x}{2}$	$\dfrac{x}{4}$	$\dfrac{x}{3}$	$\dfrac{x}{3}$	$\dfrac{x}{3}$	$\dfrac{x}{3}$
Seq.	y_s	$\dfrac{y_s}{2}$	$\dfrac{y_s}{4}$	$\dfrac{y_s}{8}$	$\dfrac{y_s}{16}$	$\dfrac{y_s}{32}$	$\dfrac{y_s}{64}$
Jac.	y_j	$\dfrac{y_j}{2}$	$\dfrac{y_j}{4}$	$\dfrac{y_j}{8}$	$\dfrac{y_j}{16}$	$\dfrac{y_j}{32}$	$\dfrac{y_j}{64}$

In this particular example the system is highly nonlinear, so that the Jacobian variation at each *Newton* step is very high, and may be seen from table 2 that the implicit methods give a relative speed up below the one in the simpler case of section 8.1. According to figure 5, the relation between the oil and gas saturation L_1-error, $\|S_{\Delta t}^l - S_{\Delta t_o}^l\|_{L_1}$, and the time step for both implicit methods, allow us to conclude that, even when the discrete treatment of cross derivatives yields a natural time control in the *Newton* step, further improvements should be introduced in order to treat regions where the phase and velocity are subject to rapid changes. As a step in that direction, a local time domain griding and parallel processing is currently under study.

9. Conclusions

We apply numerical techniques to determine the essential dynamical behavior of two novel implicit formulations for the molar masses in multicomponent, multiphase
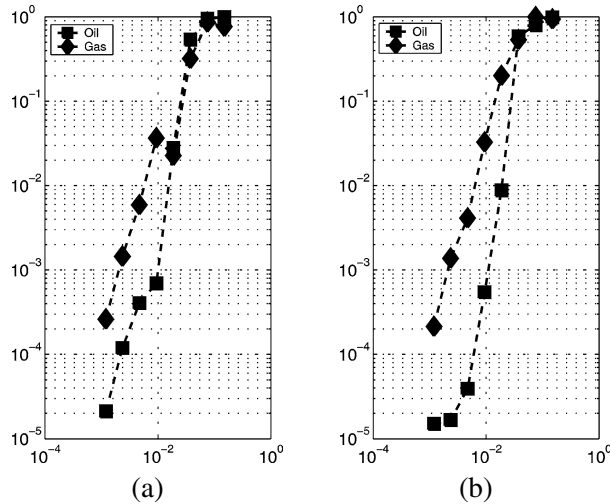
Figure 5. Athena simulation of $100y$; the L_1 error in saturations, against maximum allowed time step, $\Delta t \in (0.0012y, 0.15y)$. (a) Full Jacobian solution, and (b) sequential Jacobian.

flux in porous media. The Jacobian resulting from the *Newton–Rapson* algorithm is approximated analytically from the dew an bubble point curves. The results indicate that the size of the cross-diagonal terms in the Jacobian serve as a time step control.

Moreover it can be shown that for regions where the change in velocity and phase is small, the implicit formulation performs, in our implementation, at least a factor of 50 times faster. Hence, altogether we may conclude that both the implicit formulations for the molar mass of multicomponent, multiphase porous media exhibit a much better CPU time than the explicit solver at any time step. Besides, the error remains bounded when using a discretization-derived time step control. Some animations of these results and the C++ code for the GS–Galerkin may be found at the home-pages of the authors.

Acknowledgement

References

[1] I. Aavatsmark, T. Barkve, Ø. Bøe and T. Mannseth, Discretization on unstructured grids for inhomogeneous, anisotropic media. Part I: Derivation of the methods, SIAM J. Sci. Comput. 19(5) (1998) 1700–1716.

[2] I. Aavatsmark, T. Barkve, Ø. Bøe and T. Mannseth, Discretization on unstructured grids for inhomogeneous, anisotropic media. Part II: Discussion and numerical results, SIAM J. Sci. Comput. 19(5) (1998) 1717–1736.

[3] M. Chaib, G.E. Fladmark and M. Espedal, Implicit treatment of molar mass equations in secondary oil migration, Comput. Visual. Sci. 4(3) (2002) 191–196.

 [4] A.H. Dogru et al., A parallel reservoir simulator for large-scale reservoir simulation, SPEREE 5(1) (2002) 11–23.

 [5] G.E. Fladmark, *Secondary Oil Migration. Mathematical and Numerical Modelling in SOM Simulator* (Norsk Hydro, Bergen, 1997).

 [6] V.E. Henson and U.M. Yang, Boomer AMG: A parallel algebraic multigrid solver and preconditioner, Appl. Numer. Math. 41 (2002) 155–177.

 [7] T. Lehnhäuser and M. Schäfer, Improved linear interpolation practice for finite-volume schemes on complex grids, Internat. J. Numer. Methods Fluids 38(7) (2002) 625–645.

 [8] C. Leibovici, E.H. Stenby and K. Knudsen, A consistent procedure for pseudo-component delumping, Fluid Phase Equilibria 117 (1996) 225–232.

 [9] C. Leibovici, J. Barker and D. Waché, Method for delumping the results of compositional reservoir simulation, SPE Journal 5(2) (2000) 227–235.

[10] G.Å. Øye and H. Reme, Parallelization of a compositional simulator with a Galerkin coarse/fine method, in: *Euro-Par'99*, eds. P. Amestoy et al. (Springer, Berlin, 1999) pp. 586–594.

[11] G. Qin, H. Wang, R.E. Ewing and M.S. Espedal, Numerical simulation of compositional fluid flow in porous media, in: *Numerical Treatment of Multiphase Flows in Porous Media*, eds. Z. Chen, R.E. Ewing and Z.-C. Shi (Springer, Berlin, 2000) pp. 232–243.

[12] H. Reme and G.Å. Øye, Use of local grid refinement and a Galerkin technique to study secondary migration in fractured and faulted regions, Comput. Visual. Sci. 2(2/3) (1999) 153–162.

[13] M. Slodička, A robust and efficient linearization scheme for doubly nonlinear and degenerate parabolic problems arising in flow in porous media, SIAM J. Sci. Comput. 23(5) (2002) 1593–1614.

[14] K. Stüben, Algebraic multigrid: An introduction with applications, in: *Multigrid*, eds. U. Trottenberg, C. Osterlee and A. Schüller (Academic Press, New York, 2000).

[15] J. Vovelle, Convergence of finite volume monotone schemes for scalar conservation laws on bounded domains, Numer. Math. 90(3) (2002) 563–596.

[16] E.L. Wachspress, *Iterative Solution of Elliptic Systems and Applications to the Neutron Diffusion Equations of Reactor Physics*, International Series in Applied Mathematics (Prentice-Hall, Englewood Cliffs, NJ, 1966).

[17] J.W. Watts, A compositional formulation of the pressure and saturation equations, SPE Reservoir Engineering (May 1986) 243–252.

[18] U.M. Yang, On the use of relaxation parameters in hybrid smoothers, Lawrence Livermore National Laboratory, UCRL-JC-151575 (2003) submitted to Numer. Linear Algebra Appl.